

Reversible, Fast, and Wide-Range Oxygen Sensor Based on Nanostructured Organometal Halide Perovskite

Marc-Antoine Stoeckel, Marco Gobbi, Sara Bonacchi, Fabiola Liscio, Laura Ferlauto, Emanuele Orgiu,* and Paolo Samori*

Nanostructured materials characterized by high surface–volume ratio hold the promise to constitute the active materials for next-generation sensors. Solution-processed hybrid organohalide perovskites, which have been extensively used in the last few years for optoelectronic applications, are characterized by a self-assembled nanostructured morphology, which makes them an ideal candidate for gas sensing. Hitherto, detailed studies of the dependence of their electrical characteristics on the environmental atmosphere have not been performed, and even the effect of a ubiquitous gas such as O₂ has been widely overlooked. Here, the electrical response of organohalide perovskites to oxygen is studied. Surprisingly, a colossal increase (3000-fold) in the resistance of perovskite-based lateral devices is found when measured in a full oxygen atmosphere, which is ascribed to a trap healing mechanism originating from an O₂-mediated iodine vacancies filling. A variation as small as 70 ppm in the oxygen concentration can be detected. The effect is fast (<400 ms) and fully reversible, making organohalide perovskites ideal active materials for oxygen sensing. The effect of oxygen on the electrical characteristics of organohalide perovskites must be taken into deep consideration for the design and optimization of any other perovskite-based (opto-) electronic device working in ambient conditions.

Oxygen gas is the second most common component of the Earth's atmosphere and plays a fundamental role in cellular respiration as well as in industrial processes.^[1] Therefore the design of oxygen sensors featuring high sensitivity and selectivity, fast response and long-term stability is essential in many fields of science and technology. A promising route to achieve this objective is to use nanostructured materials, i.e., materials

with at least one dimension with a characteristic length scale on the 1–100 nm scale, such as porous materials, nanowires, or nanoparticles, as active components.^[2] Thanks to their characteristic high surface-to-volume ratio, this class of materials can be extremely sensitive to specific variation in the chemical composition of their environment.^[2d,3] Precise control over materials' nanostructuring allows to attain fine tuning of materials sensitivity to a given analyte, and therefore optimization of the sensor performances.^[4] Since the pioneering work of Collins demonstrating extreme oxygen sensitivity of the electrical properties of carbon nanotubes,^[5] several other examples have been reported of oxygen sensors and related trapping engineering based on material nanostructuring. In particular, metal oxide semiconductors^[6] and carbon-based materials^[5,7] have been used as O₂ adsorbers^[8] and sensitive materials,^[9] in which the sensing mechanism is based on a dynamic exchange between adsorbed

molecules and oxygen gas taking place on an active surface. In spite of their high sensitivity, these sensors still suffer from partial irreversibility,^[10] high operating temperatures,^[11] limited working range,^[12] and low speed,^[13] which hamper their technological application.


Among nanostructured materials, solution-processed hybrid organohalide perovskites have been extensively used in the last few years as novel semiconductors for optoelectronic devices^[14] and solar cells featuring efficiencies exceeding 22%.^[15] These materials possess an ABX₃ chemical structure, in which A is an organic cation, B is typically a metal, and X a halide ion. Thanks to a suitable processing, methyl ammonium lead iodide perovskites (MAPbI₃) can feature high surface-to-volume ratio that can be exploited for different purposes, in particular for gas sensing. Indeed, recent works revealed a marked sensitivity of MAPbI₃ photophysical properties to moisture^[16] or small gas molecules^[17] such as ammonia.^[18] Focusing in particular on oxygen, its presence was reported to modify the MAPbI₃ photoluminescence (PL) and to cause a photoinduced degradation in the MAPbI₃ structure.^[19]

Moreover, organohalide perovskites are semiconductive materials with rather high charge carrier mobility,^[20] offering the possibility to obtain an electrical readout as a consequence

M.-A. Stoeckel, Dr. M. Gobbi, Dr. S. Bonacchi, Dr. L. Ferlauto, Prof. E. Orgiu,^[†] Prof. P. Samori
University of Strasbourg
CNRS, ISIS UMR 7006
8 allée Gaspard Monge, F-67000 Strasbourg, France
E-mail: emanuele.orgiu@emt.inrs.ca; samori@unistra.fr

Dr. F. Liscio, Dr. L. Ferlauto
Istituto per la Microelettronica e Microsistemi (IMM)
Consiglio Nazionale delle Ricerche (CNR)
Via Gobetti 101, 40129 Bologna, Italy

^[†]Present address: INRS-Centre Énergie Matériaux Télécommunications, 1650 Blv. Lionel-Boulet, J3X 1S2 Varennes, Québec, Canada

 The ORCID identification number(s) for the author(s) of this article can be found under <https://doi.org/10.1002/adma.201702469>.

DOI: 10.1002/adma.201702469

of variation in the ambient composition, which is the working mechanism of resistive sensors. Hitherto MAPbI₃ has never been employed as active layer in devices that can measure environmental concentration of oxygen gas through variation of an output current.

Here, we present the first example of fully reversible, fast-response oxygen sensor device based on hybrid halide perovskite MAPbI₃ thin films featuring high sensitivity in a broad range of relative oxygen concentrations at room temperature. In particular, we give experimental demonstration of (i) a 3000-fold resistance variation, when working with relative oxygen concentration from 0% up to 100%, measured through the output current of a two-terminal sensing device realized in lateral geometry, (ii) a 70 ppm detection limit at low oxygen concentration, and (iii) sensor response time below 400 ms. Moreover, the electrical performances of our sensor were found

to be directly correlated to the perovskite nanostructure. Such important aspect could be evidenced by employing two different solution-based methods to deposit MAPbI₃ thin films on SiO₂ which, unlike ITO, TiO₂, and glass, is a nonconventional substrate/bottom layer for such material. Our results are supported by a systematic characterization of our perovskite MAPbI₃ thin-films by means of scanning electron microscopy (SEM), X-ray diffraction (XRD) and PL spectroscopy.

Figure 1 shows the structural and morphological characterization of CH₃NH₃PbI₃ films obtained on Si/SiO₂ substrates via two different solution-based deposition methods—hereafter referred to as two-step (2S) and one-step (1S). In the 2S approach, a PbI₂ solution in dimethylformamide was spin coated and annealed on a UV/ozone treated Si/SiO₂ substrate, and subsequently a solution of CH₃NH₃I in isopropanol was spin coated on top of the preassembled insulating PbI₂ film

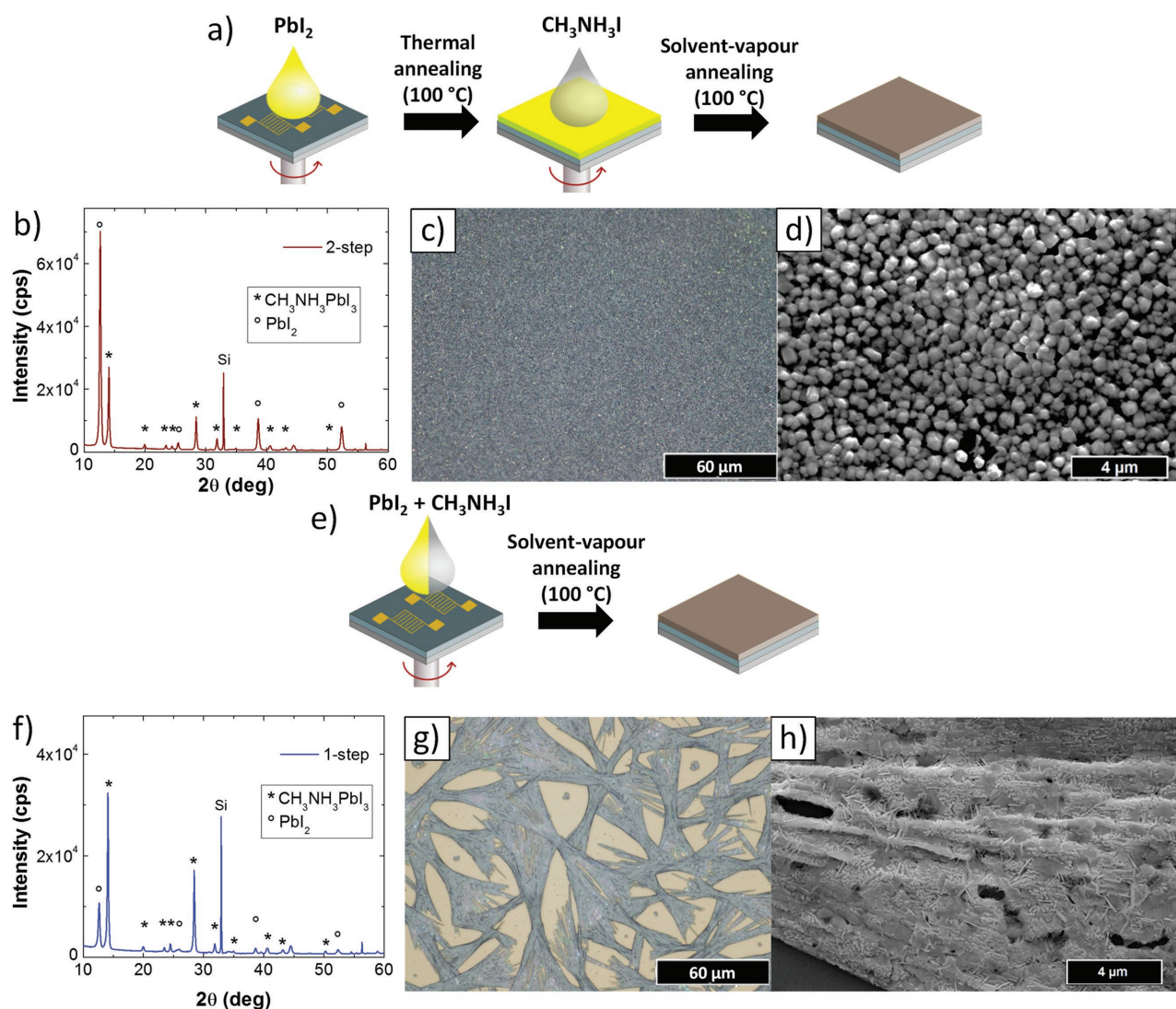


Figure 1. a) Schematics of the 2S processing method to assemble CH₃NH₃PbI₃ thin films on SiO₂. A preformed (yellow) PbI₂ film is converted into a (dark brown) CH₃NH₃PbI₃ film via spin coating of CH₃NH₃I in isopropanol. b) XRD spectra of a 2S film. c) Optical microscopy and d) SEM image of a 2S film on SiO₂ at different magnifications. e) Schematics of the 1S processing method. A solution containing both PbI₂ and CH₃NH₃I is directly spin coated onto SiO₂. f) XRD spectra of a 1S film. g) Optical microscopy and h) SEM image of a 1S film on SiO₂ at different magnifications. In (b) and (f) the peaks corresponding to CH₃NH₃PbI₃ and PbI₂ are highlighted.

(Figure 1a–d). On the contrary, in the *1S* deposition an equimolar mixture of PbI_2 and $\text{CH}_3\text{NH}_3\text{I}$ precursors was dissolved in dimethylformamide and then spin coated onto an UV/ozone treated Si/SiO₂ substrate^[21] (Figure 1d,e). In both cases, a final solvent-vapor annealing treatment at 100 °C in air for 1 h was performed to ensure the formation of the final hybrid perovskite $\text{CH}_3\text{NH}_3\text{PbI}_3$ film.^[22]

The different processing methods yield significant structural and morphological differences of the final perovskite films. XRD measurements confirm the formation of MAPbI₃ structure in both cases, but a consistent amount of PbI_2 precursor was found to be still present in *2S* samples, as highlighted by the presence of intense PbI_2 peaks in the XRD diffractogram in Figure 1b.

The film morphology was characterized by optical and scanning electron microscopy, as shown in Figure 1c,d,g,h. *2S* films are homogenous over tens of micrometers (Figure 1c) and are characterized by the presence of crystals featuring the previously reported cuboid morphology^[23] with a typical edge length of ≈ 500 nm (Figure 1d) and a thickness of ≈ 400 nm, as measured using a profilometer (see Figure S1, Supporting Information). Conversely, film preparation performed by following the *1S* procedure, lead to a nonuniform substrate coverage consisting of networks of fibril-like aggregates (Figure 1f) with thickness of ≈ 300 nm (see Figure S1, Supporting Information). A closer look into these nanostructures reveals the polycrystalline nature of the aggregates (Figure 1h). Perovskite films obtained through both methods were deposited on Si/SiO₂ substrates with prepatterned interdigitated electrodes to measure their electrical characteristics in lateral devices. Differently than in devices with a vertical geometry, in our lateral

devices the perovskite layer is fully exposed to the environment, which greatly increases the interaction with the surrounding gas molecules in the ambient.

The electrical properties of all films were recorded on samples measured inside a sealed chamber, equipped with an oxygen sensor. The devices were wired to a Keithley sourcemeter (Figure 2a). Figure 2b shows typical current–voltage (*I*–*V*) curves of *2S* devices measured at room temperature at three different oxygen concentrations: (i) nitrogen-filled chamber (below 0.1% Vol O₂), (ii) air (20.9% Vol O₂), and (iii) oxygen-filled chamber ($\approx 95\%$ Vol O₂). The device current revealed an over tenfold increase upon varying oxygen concentration from (i) to (ii) and gained almost two more orders of magnitude enhancement from (ii) to (iii). In particular, during the measurement, the electric current increased over the full range from ≈ 90 nA in (i) up to 250 μA in (iii). Moreover, Figure 2b also shows that the same resistance values could be recorded at a given O₂ concentration following repeated cycles at different oxygen/nitrogen levels inside the chamber. This experiment highlights the fully reversible character of the sensor without need of further treatments such as, for instance, a thermal annealing step in high vacuum.^[5] We highlight that the electrical response of the pristine, nonconverted PbI_2 film to oxygen is negligible, as we have demonstrated by performing a blank experiment described in Figure S2 (Supporting Information).

Analogous measurements were performed on *1S* perovskite films. Interestingly, in this case, the films would show an overall lower current passing through the junction at each gas concentration (see Figure 2c). This finding can be understood on the basis of the different morphology of the perovskite films obtained by the two processing methods. In the films obtained

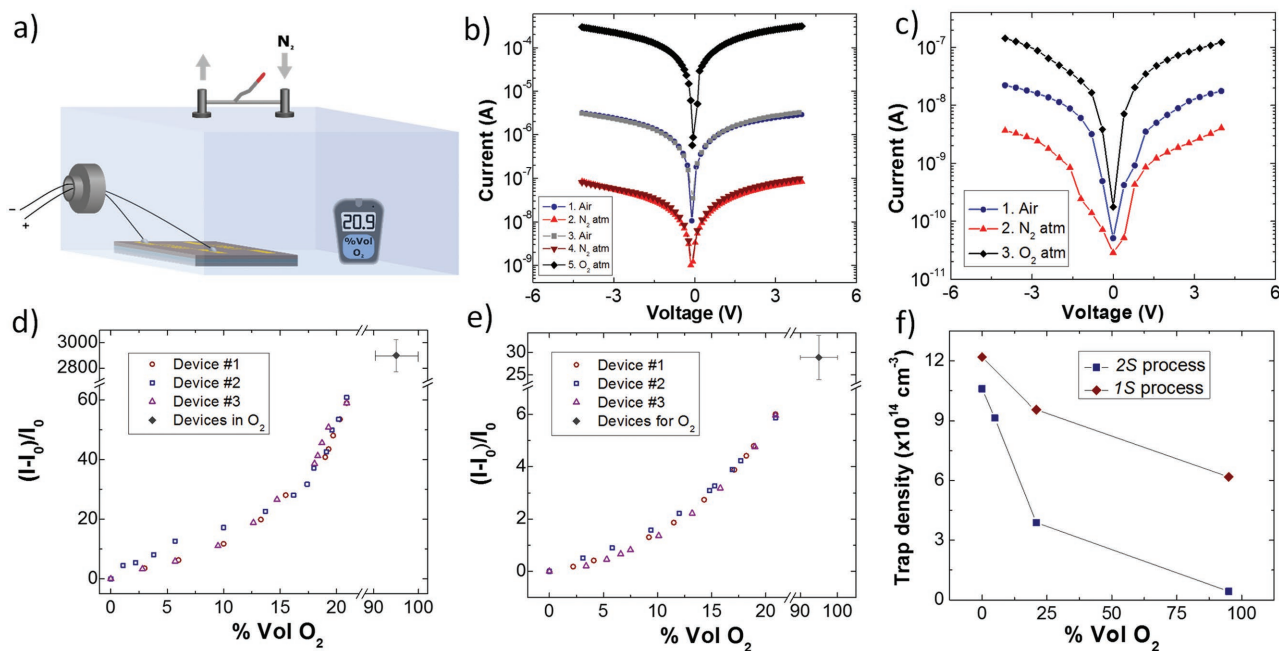


Figure 2. a) Experimental setup scheme used for device characterization. b) Current–voltage traces measured at different O₂ concentrations for the *2S* perovskite. c) Current–voltage traces measured at different O₂ concentrations for the *1S* perovskite. Sensor sensitivity versus O₂ concentration for d) *2S*, and e) *1S* perovskite, measured upon applying 4 V between the electrodes. f) Number of charge traps in the perovskite films at different oxygen concentration, as by fitting the *I*–*V* traces to the space charge limited current model.

via the 2S method, the homogeneous surface coverage limits grain boundaries between adjacent crystals, which represents a basic requirement for an efficient charge transport (see Figure 1d). Instead, films obtained via 1S method are characterized by poorly interconnected structures characterized by cracks and domain boundaries, which are detrimental for charge transport (see Figure 1h). As for the oxygen sensitivity, even in the case of the 1S films, the device current increases significantly at higher oxygen concentrations, as shown in Figure 2c. However, 1S films are less sensitive to oxygen variations, as the relative change in the electrical current is much lower than in 2S films. For the same oxygen concentrations mentioned before, the device current increased roughly four times from (i) to (ii), and a further tenfold enhancement from (ii) to (iii). A detailed evolution of the output current in a wide range of oxygen concentration (0–100%) is shown in Figure 2d,e for 2S and 1S films, respectively. In these graphs, the relative variation of output current, defined as $(I - I_0)/I_0$, is plotted, where I is the current measured at the different oxygen concentrations and I_0 is the current in pure nitrogen. Importantly, while the values displayed in Figure 2d,e were measured in three devices, they overlap onto a single curve for each deposition methods, demonstrating the high reproducibility of our sensing materials. In both cases, the current increases with oxygen concentration, as expected on the basis of the measurements shown in Figure 2b,c. In particular, in the 2S films case (Figure 2d), the ratio $(I - I_0)/I_0$ does not linearly depend on O_2 , as it increased from a value exceeding 60 in air (20.9% O_2) to almost a value of 3000 for 95% O_2 . For 1S films, current increase is up to 100 times lower than for 2S film, reaching a $(I - I_0)/I_0$ value of 27 at 95% O_2 . This finding indicates that oxygen sensing in perovskites dramatically depends on the film structure and morphology, offering the possibility to tune the sensor sensitivity by controlling the material's nanostructure via different processing methods.

The electrical study was further corroborated by optical characterization of the thin films. We have performed PL measurements on 2S and 1S films in ambient air and in N_2 , and in both cases we observe a reversible PL increase in presence of O_2 , in agreement with previous works.^[19a,24] Interestingly, even PL intensity variation is stronger in 2S films, again demonstrating the different O_2 sensitivity featured by different deposition methods (Figure S3, Supporting Information).

In order to account for the observed O_2 dependence of electrical transport and PL, we propose a trap healing mechanism according to which oxygen molecules are able to diffuse inside the perovskite crystal structure and to fill reversibly iodine vacancies that are intrinsically present inside the crystals. In turn, since iodine vacancies act as charge traps, their decreased number in presence of oxygen immediately translates into a higher number of charges available for electrical transport, i.e., higher current. In this regard, the iodine vacancies represent the sensor active sites. A similar trap healing mechanism was put forward to explain dependence of perovskite photoluminescence from O_2 concentration^[24] as well as modified Raman features upon exposure to oxygen atmosphere.^[19e] To obtain a more quantitative insight, I - V curves were recorded in devices where the external voltage was swept from 0 up to 20 V at different oxygen concentrations and analyzed them

in the framework of the space charge limited current (SCLC) model (Figure S4, Supporting Information) that allows to estimate charge trap density in semiconducting materials in two-terminal devices. The results are shown in Figure 2f for the two processing methods. In both cases, a higher number of traps is found in pure nitrogen atmosphere, while their density decreases in presence of oxygen. Moreover, we found a significantly different trap healing efficiency for the two structures. In particular, in 1S films only 50% of the traps heal upon variation of oxygen concentration from 0% to 95%, while in 2S films the healing process is extremely efficient, leading to an almost trap-free film at 95% O_2 atmosphere. This finding can be explained on the basis of the different morphologies of the perovskites obtained with the two deposition methods. In the 2S case, the crystalline domain size is very small (see Figure 1), which leads to an optimal surface-to-volume ratio that maximizes oxygen penetration in the structure. Instead, the fibril-like structures of 1S films are relatively bulky, so that oxygen is not capable of reaching the iodine vacancies buried in the bulk.

In order to confirm that the trap healing mechanism is mediated by oxygen filling of iodine vacancies, we have performed a decisive experiment. We have employed a recently developed strategy to irreversibly fill part of the iodine vacancies in a pristine perovskite film via a CH_3I treatment. As we will show, since iodine vacancies represent the active sensing sites of our perovskite-based O_2 sensors, reducing their number will result in lower sensor performances. A scheme of the reported CH_3I mediated vacancies filling is shown in Figure 3a. The iodine atom in CH_3I molecules is capable of filling an iodine vacancy while remaining attached to the CH_3 group.^[25] This mechanism is only effective for iodine vacancies very close to the perovskite surface, since the steric hindrance of CH_3I prevents its penetration into the bulk. In order to characterize the effect of the iodine vacancies filling onto the sensors performances, we measured the change in the current through a 2S film before and after the CH_3I treatment. In the pristine film, we measured a current increase by 84 times in air as compared to N_2 atmosphere (Figure 3b). After the treatment, we observe two main effects. First, the absolute current measured in pure N_2 increases from 40 to 120 nA, which can be explained as a trap healing effect induced by the CH_3I -mediated vacancy filling. Second, the sensor response to O_2 is lower, as the relative change in the current measured in N_2 and air decreases to 45 times, which can be ascribed to a lower number of active sites available for O_2 sensing. While the changes are relatively small, one should consider that only a small fraction of the iodine vacancies close to the surface are filled by the CH_3I treatment. This experiment demonstrates that iodine vacancies are indeed the active sensing sites in the perovskite layers.

However, there is an important difference between the iodine vacancies filling mechanism mediated by CH_3I gas and oxygen. While CH_3I forms covalent bonds which irreversibly passivate iodine vacancies, the O_2 mediated trap healing mechanism is reversible and in equilibrium with the O_2 concentration in the atmosphere. This property is highly beneficial, since it provides full reversibility and speed to the sensor. Figure 4a shows the real-time current of our 2S $MAPbI_3$ -based device measured by applying a constant bias of 4 V and decreasing the % of oxygen surrounding the sample from 20.9% to 7.1%. Immediately after

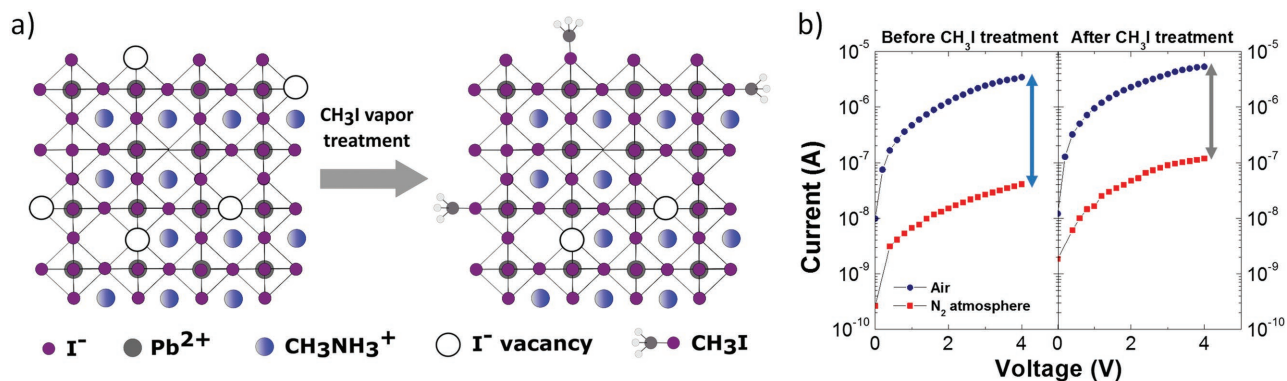


Figure 3. a) Mechanism for CH₃I iodine vacancies filling. Iodine vacancies, which are intrinsically present inside CH₃NH₃PbI₃, can be filled using CH₃I vapor. However, due to their steric hindrance, CH₃I molecules can only reach and fill vacancies close to the surface. b) Current measured in N₂ atmosphere and in air for a pristine 2S (left) and a CHI-treated film (right). We highlight that for the treated sample the absolute current in N₂ is higher, while the relative current variation is lower.

the application of a constant bias voltage, the current flowing through the perovskite layer decreases. After a short delay time (around 150 s, see Figure S5, Supporting Information) that is most likely due to the movement of ions and vacancies inside the film,^[26] the current reaches a plateau which remains stable if the O₂ concentration is not varied (see Figure S5, Supporting Information). On the contrary, sudden steps in current appear in response to variations in the O₂ concentration, as shown in Figure 4a. Moreover, a response speed of less than 400 ms has been measured (Figure 4a, inset), which represents an outstanding achievement in the field of nanostructured-based sensors operating at room temperature.^[2a,d,27] We also tested the real-time reversibility of 2S films by tuning the oxygen/nitrogen ratio flow in the chamber. Even in such broad range of oxygen exposure, our sensor shows high and fast reversibility (see Figure 4b). We then evaluated the performances of our sensor when a higher bias is applied (i.e., 30 V); interestingly, electrical current and response speed both increase of about one order of magnitude (Figure S6, Supporting Information). However, the applied electric field induces a strong deterioration of the stability of perovskite films, as can be observed on

the optical images in Figure S6c (Supporting Information), probably due to the increase of ion drift within the crystal structure.^[26] A similar experiment was performed to measure the sensor detection limit, i.e., the smallest variation of gas concentration giving rise to a detectable difference of device output current. Figure 4c shows the real-time variation of the current flowing in a 2S film in response to a 70 ppm variation in the O₂ concentration at low O₂ partial pressure. A clear step can be identified in correspondence with the O₂ increase, demonstrating that at low O₂ partial pressure the sensor sensitivity is at least 70 ppm. Finally, the selectivity of our sensors was addressed by exposing our devices to SO₂, which could compete with O₂ to fill iodine vacancies, and NH₃, which was already reported to induce a change in the electrical characteristics of CH₃NH₃PbI₃. In Figure S8 (Supporting Information), we show that the change in electrical current caused by O₂ exposure is almost three-order-of-magnitude higher than that caused by both SO₂ and NH₃, demonstrating that the response to O₂ outperforms that to other gases. Instead, the exposure of the MAPbI₃ films to water determined an irreversible degradation of the electrical performances, eventually leading to the

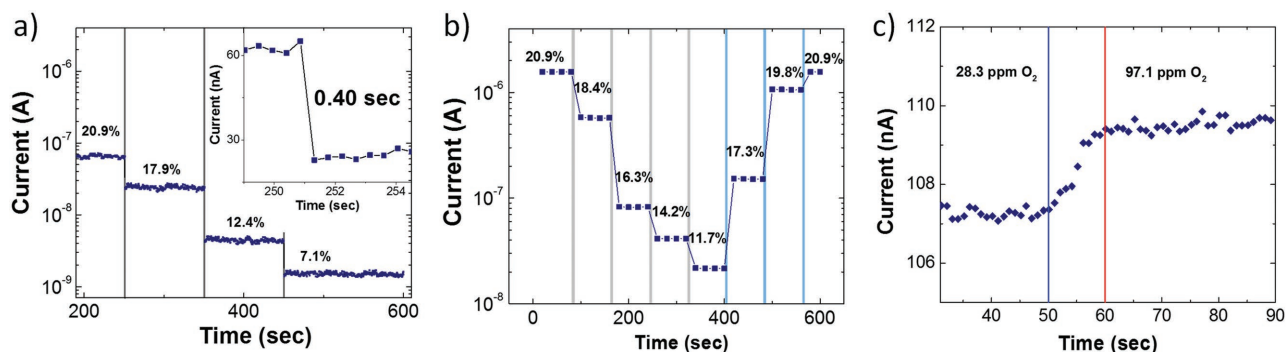


Figure 4. a) Real time change in the current measured in a 2S film in response to changes in the atmosphere composition at low bias (i.e., 4 V). Inset: speed of the sensor response. b) Reversibility of the sensor. The O₂ concentration is initially decreased from 20.9% to 11.7% and then increased back to 20.9%. In this case, measurements are performed every 20 s. c) Real-time current change corresponding to a 70 ppm O₂ variation in the sample atmosphere. The blue line indicates the instant in which oxygen gas is introduced in the chamber. After this moment, the oxygen content in the proximity of the sample increases slowly until it reaches an equilibrium state (marked by the red line).

formation of an electrically insulating specie (Figure S9, Supporting Information). It is worth noting that efficient strategies for reducing water-induced degradation are being investigated to exploit organohalide perovskites in real-life applications.^[28]

In summary, we have provided here the first experimental demonstration of the use of perovskite-based devices as O₂ sensor. We showed that device sensitivity is strongly affected by the nanoscale morphology of the perovskite films, which was controlled through the deposition method. For the most sensitive film, a more-than-three-order of magnitude increase in the current was measured by changing the atmosphere from pure N₂ to 95% O₂. The sensor response to oxygen decreases when iodine vacancies are partially filled by CH₃I, demonstrating that the measured effect stems from a dynamic trap healing mechanism mediated by oxygen filling of I vacancies, which therefore act as the active sensing sites. The device current variation was found to be very fast (400 ms) and completely reversible at room temperature, making nanostructured organohalide perovskites ideal materials for oxygen sensing, and paving the way to so-far unexplored applications of this class of materials. Moreover, the effect of oxygen on the electrical characteristics of MAPbI₃ must be taken into deep consideration for the design and optimization of any other perovskite-based (opto-) electronic device working in ambient conditions. Our results anticipate that postdeposition oxygen treatments and optimization of the device atmosphere might further contribute to the development of this class of materials.

Experimental Section

Preparation Procedure of the Perovskite Films: For the 2S method, 100 μL of a solution of PbI₂ (461 mg mL⁻¹ in dimethylformamide (DMF)) were spin coated on the substrate at 3000 rpm (500 rpm s⁻¹, 11 s) then 6000 rpm (500 rpm s⁻¹, 11 s), followed by an annealing at 100 °C for 5 min. A second step was to spin coat 100 μL of a solution of CH₃NH₃I (15 mg mL⁻¹ in propan-2-ol) on the PbI₂ layer at 4000 rpm (500 rpm s⁻¹, 40 s).

For the 1S method, 100 μL of a mixed solution of PbI₂ (461 mg mL⁻¹) and CH₃NH₃I (154 mg mL⁻¹) in DMF were spin coated on the substrate 4000 rpm (2000 rpm s⁻¹, 30 s).

The perovskite films were completed by a solvent annealing at 100 °C for 1 h under a petri dish with 15 μL of DMF and stored inside a glovebox filled with nitrogen gas.

Iodine Vacancies Passivation by Methyl iodide: The MAPbI₃ films were treated on a hot plate at 40 °C under a petri dish with 10 μL of CH₃I for 10 min.

Oxygen Sensor Characteristics: The oxygen sensor used is a Dräger Pac 5500 O₂ with a detection range between 0% and 25% Vol and a resolution of 0.1% Vol.

Device Fabrication and Characterization: In order to prepare samples, SiO₂/Si-n⁺⁺ substrates 230 nm thick SiO₂ (from Fraunhofer Institute for Photonic Microsystems IPMS, Dresden, Germany) were cleaned in an ultrasonic bath of acetone then propan-2-ol. The substrates were then gently dried with a nitrogen flow. By using a shadow mask, 3 nm of chromium then 47 nm of gold were thermally evaporated on them with a Plassys MEB 300, forming interdigitated electrodes with a constant width of 10 nm and variable length from 60 to 120 μm. The substrates are then UV-O₃ treated for 5 min following 25 min of incubation. The devices were measured in dark to avoid any photocurrent effect or photodegradation related to the presence of light and oxygen.^[19b,d] The variation of the electrical resistance of the perovskite sensor to environmental changes in the low-concentration regime of O₂ content

was measured in a nitrogen filled glovebox. A base oxygen pressure of 28 ppm was controllably increased up to ≈97 ppm.

Supporting Information

Supporting Information is available from the Wiley Online Library or from the author.

Acknowledgements

This work was supported by the EC through the Marie Skłodowska-Curie ITN project iSwitch (GA-642196), the ERC project SUPRAFUNCTION (GA-257305), the FET project UPGRADE (GA-309056), and Marie Curie IEF GALACTIC (PIEF-GA-2013-628563), the Agence Nationale de la Recherche through the LabEx project Chemistry of Complex Systems (ANR-10-LABX-0026_CSC), and the International Center for Frontier Research in Chemistry (icFRC).

Conflict of Interest

The authors declare no conflict of interest.

Keywords

hybrid organohalide perovskites, nanostructured materials, oxygen sensors, trap density

Received: May 3, 2017
Revised: June 15, 2017
Published online: July 25, 2017

- [1] a) I. Linnerud, P. Kaspersen, T. Jaeger, *Appl. Phys. B: Lasers Opt.* **1998**, *67*, 297; b) H. Zhu, H. F. Bunn, *Science* **2001**, *292*, 449.
- [2] a) R. Meyer, R. Waser, *Sens. Actuators, B* **2004**, *101*, 335; b) E. S. Cho, J. Kim, B. Tejerina, T. M. Hermans, H. Jiang, H. Nakanishi, M. Yu, A. Z. Patashinski, S. C. Glotzer, F. Stellacci, B. A. Grzybowski, *Nat. Mater.* **2012**, *11*, 978; c) E. Steven, V. Lebedev, E. Laukhina, C. Rovira, V. Laukhin, J. S. Brooks, J. Veciana, *Mater. Horiz.* **2014**, *1*, 522; d) J. Zhang, X. Liu, G. Neri, N. Pinna, *Adv. Mater.* **2016**, *28*, 795.
- [3] F. K. Perkins, A. L. Friedman, E. Cobas, P. M. Campbell, G. G. Jernigan, B. T. Jonker, *Nano Lett.* **2013**, *13*, 668.
- [4] a) M. C. McAlpine, H. Ahmad, D. Wang, J. R. Heath, *Nat. Mater.* **2007**, *6*, 379; b) N. Liu, M. L. Tang, M. Hentschel, H. Giessen, A. P. Alivisatos, *Nat. Mater.* **2011**, *10*, 631.
- [5] P. G. Collins, *Science* **2000**, *287*, 1801.
- [6] a) D. E. Williams, *Sens. Actuators, B* **1999**, *57*, 1; b) N. Barsan, D. Koziej, U. Weimar, *Sens. Actuators, B* **2007**, *121*, 18.
- [7] a) J. Kong, N. R. Franklin, C. W. Zhou, M. G. Chapline, S. Peng, K. J. Cho, H. J. Dai, *Science* **2000**, *287*, 622; b) F. Schedin, A. K. Geim, S. V. Morozov, E. W. Hill, P. Blake, M. I. Katsnelson, K. S. Novoselov, *Nat. Mater.* **2007**, *6*, 652; c) D. R. Kauffman, A. Star, *Angew. Chem., Int. Ed.* **2008**, *47*, 6550; d) J. D. Fowler, M. J. Allen, V. C. Tung, Y. Yang, R. B. Kaner, B. H. Weiller, *ACS Nano* **2009**, *3*, 301; e) W. Yuan, G. Shi, *J. Mater. Chem. A* **2013**, *1*, 10078.
- [8] M. Setvin, U. Aschauer, P. Scheiber, Y. F. Li, W. Hou, M. Schmid, A. Selloni, U. Diebold, *Science* **2013**, *341*, 988.
- [9] H. C. Lee, W. S. Hwang, *Mater. Trans.* **2005**, *46*, 1942.

- [10] J. Eriksson, V. Khranovskyy, F. Soderlind, P. O. Kall, R. Yakimova, A. L. Spetz, *Sens. Actuators, B* **2009**, *137*, 94.
- [11] L. Yao, G. Ou, W. Liu, X. Zhao, H. Nishijima, W. Pan, *J. Mater. Chem. A* **2016**, *4*, 11422.
- [12] P. Jasinski, T. Suzuki, H. U. Anderson, *Sens. Actuators, B* **2003**, *95*, 73.
- [13] a) G. Neri, A. Bonavita, G. Micali, G. Rizzo, S. Galvagno, M. Niederberger, N. Pinna, *Chem. Commun.* **2005**, 6032; b) A. Gurlo, *ChemPhysChem* **2006**, *7*, 2041.
- [14] a) A. Kojima, K. Teshima, Y. Shirai, T. Miyasaka, *J. Am. Chem. Soc.* **2009**, *131*, 6050; b) J. Burschka, N. Pellet, S. J. Moon, R. Humphry-Baker, P. Gao, M. K. Nazeeruddin, M. Grätzel, *Nature* **2013**, *499*, 316; c) G. Xing, N. Mathews, S. S. Lim, N. Yantara, X. Liu, D. Sabba, M. Grätzel, S. Mhaisalkar, T. C. Sum, *Nat. Mater.* **2014**, *13*, 476; d) Z. K. Tan, R. S. Moghaddam, M. L. Lai, P. Docampo, R. Higler, F. Deschler, M. Price, A. Sadhanala, L. M. Pazos, D. Credgington, F. Hanusch, T. Bein, H. J. Snaith, R. H. Friend, *Nat. Nanotechnol.* **2014**, *9*, 687; e) Y. Lee, J. Kwon, E. Hwang, C. H. Ra, W. J. Yoo, J. H. Ahn, J. H. Park, J. H. Cho, *Adv. Mater.* **2015**, *27*, 41; f) W. S. Yang, J. H. Noh, N. J. Jeon, Y. C. Kim, S. Ryu, J. Seo, S. I. Seok, *Science* **2015**, *348*, 1234; g) X. Li, D. Bi, C. Yi, J. D. Decoppet, J. Luo, S. M. Zakeeruddin, A. Hagfeldt, M. Grätzel, *Science* **2016**, *353*, 58.
- [15] Photovoltaic Research | NREL, <https://www.nrel.gov/pv/> (accessed: April 2017).
- [16] W. Xu, F. Li, Z. Cai, Y. Wang, F. Luo, X. Chen, *J. Mater. Chem. C* **2016**, *4*, 9651.
- [17] H. H. Fang, S. Adjokatse, H. Wei, J. Yang, G. R. Blake, J. Huang, J. Even, M. A. Loi, *Sci. Adv.* **2016**, *2*, e1600534.
- [18] a) Y. Zhao, K. Zhu, *Chem. Commun.* **2014**, *50*, 1605; b) C. Bao, J. Yang, W. Zhu, X. Zhou, H. Gao, F. Li, G. Fu, T. Yu, Z. Zou, *Chem. Commun.* **2015**, *51*, 15426.
- [19] a) J. F. Galisteo-Lopez, M. Anaya, M. E. Calvo, H. Miguez, *J. Phys. Chem. Lett.* **2015**, *6*, 2200; b) N. Aristidou, C. Eames, I. Sanchez-Molina, X. Bu, J. Kosco, M. S. Islam, S. A. Haque, *Nat. Commun.* **2017**, *8*, 15218; c) Y. Tian, M. Peter, E. Unger, M. Abdellah, K. Zheng, T. Pullerits, A. Yartsev, V. Sundstrom, I. G. Scheblykin, *Phys. Chem. Chem. Phys.* **2015**, *17*, 24978; d) H. Yuan, E. Debroye, K. Janssen, H. Naiki, C. Steuwe, G. Lu, M. Moris, E. Orgiu, I. H. Uji, F. De Schryver, P. Samori, J. Hofkens, M. Roeloffs, *J. Phys. Chem. Lett.* **2016**, *7*, 561; e) W. Kong, A. Rahimi-Iman, G. Bi, X. Dai, H. Wu, *J. Mater. Chem. C* **2016**, *120*, 7606; f) X. Fu, D. A. Jacobs, F. J. Beck, T. Duong, H. Shen, K. R. Catchpole, T. P. White, *Phys. Chem. Chem. Phys.* **2016**, *18*, 22557; g) H. Yuan, E. Debroye, G. Caliandro, K. P. Janssen, J. van Loon, C. E. Kirschhock, J. A. Martens, J. Hofkens, M. B. Roeloffs, *ACS Omega* **2016**, *1*, 148.
- [20] Q. Dong, Y. Fang, Y. Shao, P. Mulligan, J. Qiu, L. Cao, J. Huang, *Science* **2015**, *347*, 967.
- [21] R. Munir, A. D. Sheikh, M. Abdelsamie, H. Hu, L. Yu, K. Zhao, T. Kim, O. E. Tall, R. Li, D. M. Smilgies, A. Amassian, *Adv. Mater.* **2017**, *29*, 1604113.
- [22] G. Divitini, S. Cacovich, F. Matteocci, L. Cinà, A. Di Carlo, C. Ducati, *Nat. Energy* **2016**, *1*, 15012.
- [23] J. H. Im, I. H. Jang, N. Pellet, M. Grätzel, N. G. Park, *Nat. Nanotechnol.* **2014**, *9*, 927.
- [24] Y. Tian, A. Merdasa, E. Unger, M. Abdellah, K. Zheng, S. McKibbin, A. Mikkelsen, T. Pullerits, A. Yartsev, V. Sundström, I. G. Scheblykin, *J. Phys. Chem. Lett.* **2015**, *6*, 4171.
- [25] W. Xu, J. A. McLeod, Y. Yang, Y. Wang, Z. Wu, S. Bai, Z. Yuan, T. Song, Y. Wang, J. Si, R. Wang, X. Gao, X. Zhang, L. Liu, B. Sun, *ACS Appl. Mater. Interfaces* **2016**, *8*, 23181.
- [26] Z. Xiao, Y. Yuan, Y. Shao, Q. Wang, Q. Dong, C. Bi, P. Sharma, A. Gruverman, J. Huang, *Nat. Mater.* **2015**, *14*, 193.
- [27] K. Rajavel, M. Lalitha, J. K. Radhakrishnan, L. Senthilkumar, R. T. Rajendra Kumar, *ACS Appl. Mater. Interfaces* **2015**, *7*, 23857.
- [28] Q. Tai, P. You, H. Sang, Z. Liu, C. Hu, H. L. Chan, F. Yan, *Nat. Commun.* **2016**, *7*, 11105.